ANL/MSD/CP-95844

58918-00-105
58930-00-105
58712-00-105

Stresses in Thermally Grown Alumina Scales Near Edges and Corners

M. Grimsditch,[*] D. Renusch,[*#] B. Veal,[*] J.K. Wright,[‡] and R.L. Williamson[‡]

[*]*Materials Science Division, Argonne National Laboratory, Argonne, IL 60439*

[#]*Western Michigan University; Kalamazoo, MI 49008*

[‡]*Idaho National Engineering Laboratory, Idaho Falls, ID 83415*

Proceedings of 193rd Meeting of the Electrochemical Society, San Diego, CA, May 3-8, 1998

This work supported by the U.S. Department of Energy, Basic Energy Sciences-Material Sciences under contract #W-31-109-ENG-38.

DISCLAIMER

DISCLAIMER

Portions of this document may be illegible in electronic image products. Images are produced from the best available original document.

STRESSES IN THERMALLY GROWN ALUMINA SCALES NEAR EDGES AND CORNERS

M. Grimsditch,* D. Renusch*†, B. W. Veal,* J.K. Wright+ and R.L. Williamson.+

*Argonne National Laboratory, Argonne, IL 60439, USA
†Western Michigan University, Kalamazoo, MI 49008, USA
+Idaho National Engineering Laboratory, Idaho Falls, ID 83415, USA

Abstract

We have investigated the residual stress near edges and corners of thermally grown alumina scales. Micro fluorescence measurements, performed on alloys with composition Fe-5Cr-28Al (at.%, bal. Fe) oxidized at 900° C, showed a large (>50%) reduction in hydrostatic stress in the vicinity of edges and corners. Surprisingly, stress relaxation persists out to distances ten times the scale thickness from the edge. Finite element analysis calculations confirm the experimental results and provide a considerably more detailed picture of the stress distribution and its components.

I. Introduction

Thermally grown alumina scales play an extremely important role in providing protection against environmental attack, especially in high temperature (T > 1000° C) oxidizing environments. Whereas desirable scales are stable, slow growing and self healing, all scales ultimately fail when operated in corrosive environments at extreme temperatures. For a truly protective scale, failure only occurs when the alloy is depleted of the scale-forming element.[1] Accelerated chemical attack can of course greatly reduce the lifetime, [2] but very often, scales fail prematurely by cracking or spalling particularly under thermal cycling conditions. The driving force for these failures is the stress that develops within the scale in response to the oxide growth process, [3] the thermal expansion mismatch between the oxide and the substrate, and any phase transformation that may occur in the scale or in the alloy. To develop an understanding of the scale failure processes, and in order to develop ways of preventing them, it is important to obtain reliable methods for measuring stresses in the scales and for detecting the onset of scale failure.

Although the ruby fluorescence has been used for decades as a stress indicator in diamond anvil cells [4] only recently has it been used to measure the stress levels in thermally grown oxide scales. [5-14] It is well known that the Cr impurities in α-Al_2O_3 produce the characteristic R-line fluorescence doublet at 6943 Å and 6929 Å. It is also known that the frequency of the fluorescence changes as a function of the stress applied to the host material. Details relating the shift to average stress and or strain in a polycrystalline material can be found in the literature. [9, 15-22] For the sake of this work it is sufficient to recall that the average hydrostatic stress σ_H (one third of the trace of the stress tensor) is related to the shift in frequency $\Delta\nu$ by

$$\sigma_H = 0.133\ \Delta\nu \qquad (1)$$

when $\Delta\nu$ is expressed in cm^{-1} and σ_H in GPa.[4] By calculating the hydrostatic stress (Eq. 1) the only assumption is that the crystallites in the scale have no preferred orientation.

The techniques and instrumentation normally used for recording the fluorescence are the same as those used in Raman spectroscopy. It is not surprising therefore that, like Raman scattering, fluorescence studies can be performed with the same very high spatial resolution as that available in micro-Raman investigations. Typically this type of equipment consists of a microscope interfaced to a spectrometer; our particular instrument allowed us to focus the incident laser beam down to ≈2 microns and to collect the fluorescence from the illuminated region. This high spatial resolution has allowed us to investigate the stress field surrounding a surface convolution.[23] Here we present our investigation of stress profiles near scale edges and corners. For the purpose of this study an edge is the intersection of two flat orthogonal surfaces and a corner is the intersection of three such surfaces.

Stress distributions close to edges are of particular interest because spallation and debonding often seem to occur in their vicinity[24,25]; this is often interpreted as an indication that edges are regions of stress concentration. However, the large number of possible contributions to residual-stress accumulation and relaxation (growth strains, thermal expansion mismatch, creep, phase transformations, debonding, cracking etc.) make an a priori treatment of this phenomenon complex. It is especially difficult to make initial assumptions regarding which effects are likely to contribute most strongly in a given instance. The experimental data now available with the micro-fluorescence technique offer the possibility of testing the results of model calculations. In the present study we compare our experimental results with finite element analysis.[24] The measurements provide verification of, and confidence in, the model, while the model provides the detailed information necessary for an improved understanding of failure prediction and design improvements.

II. Experimental Details and Results

The samples were coupons of Fe-5Cr-28Al (at.%, bal Fe) with dimensions (4.50 ± 0.02 by 4.85 ± 0.03 mm) with thickness (127, 254, 508, and 940 μm). All six faces of each sample were polished with 1 micron diamond polishing grit. The samples were oxidized in air at 900°C for two hours. After heat treatment the fluorescence was measured at room temperature. The scale thickness was obtained from the interference patterns of reflected visible light resulting from the contributions from the air-oxide and metal-oxide surfaces. Fluorescence spectra were recorded in both macro- and micro- configurations. In the macro experiments the incident beam was focused down to a spot size of about 75 μm and the scattered light was collected along the surface normal with an f/1.4 lens. The micro fluorescence spectra were acquired in the back scattering geometry through a microscope which allowed the laser to be focused to about 2 μm. In both cases the signal originates from the entire scale thickness.

Figure 1 is a schematic view of a corner of one of the oxidized samples described above. The black dots are the positions on the surface where micro-fluorescence spectra were recorded. The arrows identify the location on the sample where the two spectra in Fig

2, labeled 1 and 2, were acquired. Figure 2 clearly shows that spectrum 1, taken closer to the edge, has a shorter wavelength, and therefore a lower hydrostatic stress. To obtain peak positions, the spectra in Fig 2 were fitted with two Lorentzians and a quadratic background shown by the full lines in the figure. Also shown in Fig 2 is a ruby spectrum from an unstrained single crystal.

The behavior close to an edge and a corner is exhibited in Fig 3 where we plot the hydrostatic stress as a function of distance from the corner along the corner diagonal, and as a function of distance from an edge corresponding to lines C and B respectively (Fig. 1). Fig. 3 shows that, at the corner, the hydrostatic stress is approaching zero indicating that there is nearly complete relaxation of the hydrostatic stress. Anticipating the comparison with calculations to be presented later, we emphasize that all our stress determinations were made on the flat surface of the sample; we did not attempt to probe the very-near-edge region where the sample is rounded. This rounded portion, where two faces meet, is comparable in size to our laser spot and hence we do not have the necessary resolution to probe it in detail.

III. Model calculations

A. Approach

Finite element analysis (FEA) is extensively applied to analyze structures in which non-homogeneous stress and strain fields result as a consequence of complex geometrical structures and loading conditions. The method deals with the complexities by dividing the 'structure' into smaller geometrically simple subsections (elements) for which the governing partial differential equations can be approximated by algebraic equations. A combination or assembly of the elements results in a system of algebraic equations that are readily solved on a computer. The solution typically involves an iterative procedure in which the displacements (and thus stress and strain) in each element are adjusted to satisfy the boundary conditions.

The assumptions made in modeling the residual stresses are as follows: The oxide and substrate are perfectly bonded throughout the calculation, and the specimen begins in a stress free condition at 900°C. Stresses or deformation resulting from growth of the oxide are not considered; growth stresses are thought to be small relative to thermally generated stresses [5]. All material properties are assumed to be homogeneous and isotropic, and were obtained from tabulations for bulk materials, as reported previously [25]. Elastic properties are assumed to be independent of temperature [26, 27], but monotonic temperature-dependent expansion coefficients [28, 29] are used for both materials. These latter assumptions are equivalent to precluding phase transformations in both the substrate and oxide. Plasticity effects were precluded for the scale; the alloy was assumed to be governed by a von Mises yield condition and isotropic hardening with temperature-dependent plastic flow curves, based on tensile curves of an Fe-28Al-2Cr alloy [30].

Cooling is assumed to be spatially uniform and relatively rapid, so time-dependent deformation (creep) is not considered. A two-dimensional computational mesh [25] was used to model the samples in generalized plane strain. The mesh has a nominal edge length of 100 μm and a uniform 0.5 μm thick oxide scale on the entire exterior. Rather than a sharp edge where two surfaces meet, a corner radius of 2 μm was used.

B. Results

When the specimen is cooled from an oxidation temperature to ambient, a biaxial stress state (In a reference frame with y along the surface normal $\sigma_{xx}=\sigma_{zz}$, $\sigma_{yy}=0$) exists in regions distant from the edges, with stress and strain values essentially equivalent to infinite plate solutions. The film is in compression and the substrate in tension because of the difference in thermal contraction of the two materials. At an edge, however, a type of bending phenomenon is observed in the film. The substrate plasticity enables it to significantly deform to accommodate stresses, and the film near the corner behaves similarly to an elastic beam in bending, with tensile stresses present along the outside of the beam and compressive stresses on the inside of the beam. The resultant stress state is the sum of this stress gradient from bending and the compression throughout the film from thermal contraction. The modeling results are very similar to those reported in detail earlier for an axisymmetric cylinder [25] and vary with the scale thickness, radius of curvature, and substrate plasticity.

The average hydrostatic stress across the scale, determined as a function of distance from the edge, is compared with measured stresses in Fig 4. The symbols correspond to averages of experimental measurements acquired along multiple traces perpendicular to the sample edge (such as line A in Fig 1). The full and dashed lines are the result of the model FEA calculations and were first volume averaged through each column of elements in the scale, consistent with the fact that the oxides are relatively transparent and the entire scale thickness is probed experimentally. The dashed line in Fig. 4 stems from a calculation where only elastic deformation was allowed; since it does not reproduce the experimentally observed decay length, we conclude that it is necessary to include plastic derformation in the substrate. The full line in Fig. 4 represents calculations including plastic deformation. Agreement with experiment, both the shape of the curves and the stress magnitudes, is excellent.

IV. Discussion

The process of depth averaging the calculated results shown in Fig. 4, necessary in order to compare with experiment, does involve some loss of information. Far from an edge the stress gradients are relatively small and hence the averaging has little effect. Close to the edge, however, rich stress patterns, apparent in the calculations, are lost during the averaging. Local tensile stress components are calculated at the edge, so although the measured hydrostatic stress appears to be approaching zero near the edge, this cannot be taken as an indication that damage is unlikely.

With the above understanding of what the measured stress actually represents, it is useful to view the apparent hydrostatic stress relaxation in simple qualitative terms. It was shown in Ref. 9 that the stress on a flat surface of these alloys is well described by an in-plane biaxial stress ($\sigma_{xx} = \sigma_{zz}$) with the stress along the surface normal being zero ($\sigma_{yy} = 0$). On the y surface, as the x face is approached, one may guess that the σ_{XX} stress may relax. We may then expect

$$\sigma_{xx} = \sigma_{xx}(\infty)\ (1 - \exp\{-d_x/L\}) \qquad (2)$$

where $\sigma_{XX}(\infty)$ is the stress far from the edge, d_X is the distance from the edge, and L is a characteristic decay length. The hydrostatic stress is given by

$$\sigma_H = \sigma_H(\infty)\,(1 - 0.5\exp\{-d_x/L\} - 0.5\exp\{-d_z/L\}) \qquad (3)$$

where d_X and d_Z are the distances from the x and z edges respectively.

The full lines in Fig. 3 are a least squares fit of Eq 3 to the edge and corner data along lines B and C in Fig 1; the fit parameters are L = 4.8 μm and $\sigma_H(\infty)$ =- 4.1 GPa. We can see that the above expression describes the roughly 50% drop in the average σ_H as an edge is approached, the almost zero stress close to a corner, and the overall shape of the results in Fig. 3. It does not provide any insight into the origin of the relaxation nor of the decay length L; both of these issues require the more sophisticated FEA approach described above.

The usefulness of Eq. 3 is not that it allows us to mimic the full FEA calculations, but that it allows us to predict the hydrostatic stress at a corner. The large number of elements needed in an FEA calculation to describe a three dimensional object makes such calculations computationally intensive. The above expession should prove useful to estimate the stresses in such cases.

The decay length is determined by: the geometry of the scale at the edge, and by the substrate plasticity and concomitant bending of the scale. An FEA for the same geometry and computational mesh but with no plasticity produces virtually no bending and the changes in both σ_H and σ_{XX} from their value far from the edge are smaller and extend only a short distance from the edge (dashed line in Fig 4).

V. Summary and Conclusions

High-resolution ruby fluorescence measurements have enabled stress determination in an oxide scale near the sample edge. A relaxation of the average hydrostatic stress, which extends more than ten times the scale thickness, is observed experimentally as the edge is approached.

FEA modeling is in good agreement with these stress measurements and shows that hydrostatic stress relaxation is the result of both the geometry of the edge and the degree of substrate plasticity.

Modeling also indicates that while measured compressive stresses decrease in magnitude as the edge is approached, local stresses can increase, but may not be detected experimentally because the measured stresses are hydrostatic and and are averaged through the thickness of the scale. The highest local stresses, including tensile stresses that constitute the greatest potential for damage, are predicted in the region of curvature where experimental stress data could not be gathered.

The ruby fluorescence and FEA methods work well in concert. The measurements provide verification of and confidence in the model, and the model provides the detailed

information necessary for improved understanding, failure prediction, and design improvements. A simple phenomenological model is proposed that reproduces the FEA calculations and allows predictions to be made in three dimensional situations not easily amenable to FEA.

Acknowledgments

Work at ANL supported by the US Department of Energy, BES Materials Sciences under contract W-31-109-ENG-38.

REFERENCES

1 W. J. Quadakkers and M. J. Bennett, Mat. Sci. and Tech., 10, 126 (1994)
2 H. J. Grabke, J. F. Norton and F. G. Casteels, in High Temperature Alloys for Gas Turbines and Other Applications, Vol I, W. Betz, ed. (Reidel, Dordrecht, 1986) p 254.
3 J. Stringer, Corr. Sci 10, 513 (1970).
4 A. Jayaraman. Rev. Mod. Phys. 55, 65 (1983).
5 K. Natesan, B. W. Veal, M. Grimsditch, D. Renusch and A. P. Paulikas, Proc. Ninth Annual Conference on Fossil Energy Materials, Oak Ridge, TN, CONF-9505204, ORNL/FMP-95/1, p. 225 (1995)
6 K. Natesan, C. Richier, B. W. Veal, M. Grimsditch, D. Renusch and A. P. Paulikas, Argonne National Laboratory Report ANL/FE-95/02 (1995)
7 K. Natesan, K. L. Klug, D. Renusch, M. Grimsditch and B. W. Veal, Tenth Annual Conference on Fossil Energy Materials, Knoxville TN, May 14-16, 1996.
8 D. Renusch, B. W. Veal, I. Koshelev, K. Natesan, M. Grimsditch and P. Y. Hou, Proc. of Spring Meeting of Materials Research Soc., San Francisco CA, 1996. Vol 436, Thin Films: Stresses and Mechanical Properties VI, p 511; and Proc. 190th ECS fall meeting, San Antonio, TX,. 1996. Vol 96-26, Fundamental Aspects of High Temperature Corrosion, ed by D. A. Shores, R. Rapp and P. Y. Hou, Electrochem. Soc.,Pennington, NJ 1997. p 62.
9 D. Renusch, M. Grimsditch, I. Koshelev, B. W. Veal, Oxidation of Metals **48**, 469 (1997)
10 D. M. Lipkin, D. R. Clarke, M. Hollatz, M. Bobeth, W. Pompe, Corrosion Science, **39**, 231, (1997)
11 D. M. Lipkin, H. Schaffer, F. Adar, D. R. Clarke, Appl. Phys. Lett, **70**, 2550, (1997)
12 C. Mennicke, E. Schumann, C. Ulrich and M. Ruhle, (presented at the 4th Int. Symp. on High Temp. Corrosion and Protection of Mat., Les Embiez, France, May 20-24, 1996) to be published in Mater. Sci. Forum.
13 D. M. Lipkin and D. R. Clarke, Oxidation of Metals 45, 267 (1996).
14 R. J. Christennsen, D. M. Lipkin, D. R. Clarke, Acta Materialia, **44**, 3813 (1996)
15 Q. Wen, D. R. Clarke, N. Yu and M,. Nastasi, Appl. Phys. Lett. **66**, 293 (1995).
16 J. He and D. R. Clarke, J. Am. Ceram. Soc.**78**, 1347 (1995).
17 Qing Ma and D. R. Clarke, J. Am. Ceram. Soc.**77**, 298 (1994).
18 Qing Ma and D. R. Clarke, J. Am. Ceram. Soc.**76**, 1433 (1993).
19 Qing Ma, and D. R. Clarke, Acta metall. mater. Vol **41**, No. 6, 1811 (1993).

20 Qing Ma, W. Pompe, J. D. French, D. R. Clarke, Acta metall. mater. Vol **42**, No. 5, 1673 (1994).
21 S. E. Molis and D. R. Clarke, J. Am. Ceram. Soc.**73**, 3189 (1990).
22 Qing Ma and D. R. Clarke, The American Society of Mechanical Eneineers, AMD-Vol **181**, Book No. H00888 - 1993
23 J. K. Wright, R. L. Williamson, D. Renusch, B. Veal, M. Grimsditch, P. Y. Hou, R. M. Cannon. To be published
24 R. L. Williamson, J. K. Wright and R. M. Cannon, 190th ECS fall meeting, Oct. 6-11, 1996, San Antonio, TX. To be published in Fundamentals of High Temperature Corrosion VI, ed by D. A. Shores and P. Y. Hou, Electrochem. Soc., Pennington, PA 1997.
25 J. K. Wright, R. L. Williamson and R. M. Cannon, Materials Science and Enginerring **A230** 202 (1997)
26 W. J. Lackey, D. P. Stinton, G. A. Carny, L. L. Fehrenbacher, A. C. Schaffhauser, Ceramic coatings for heat engines materials-status and future needs, Oak Ridge National Laboratory Report ORNL/TM-8959, 1984
27 P. Morgand, P. Mouturat, G. Sainfort, Acta Metallurgica 16 (1968) 867
28 K. B. Alexander, K. Prüssner, P. Y. Hou and P. F. Tortorelli, Proc. of the 3rd Int. Conf. on Microscopy of Oxidation, Cambridge, UK Sept. 16-18, 1996.
29 P. Y. Hou, Z. R. Shui, G. Y. Chuang and J. Stringer, J. Electrochem. Soc. 139, 1119 (1992).
30 J. R. Knibloe, R. N. Wright, V. K. Sikka, R. H. Baldwin, C. R. Howell, Materials Science and Engineering A153 (1992) 382

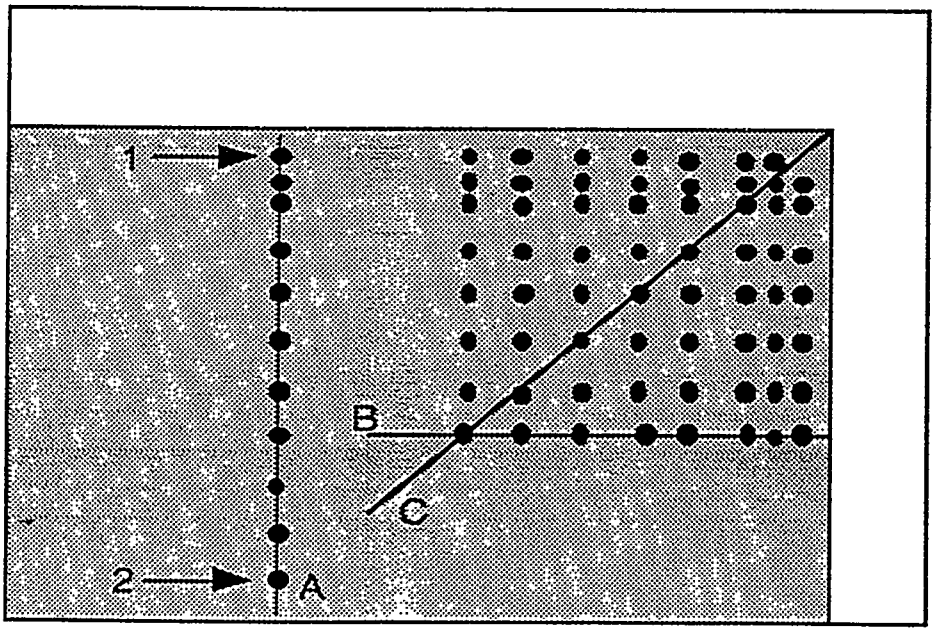

Fig 1 Schematic diagram of the spots near the corner of a sample at which ruby spectra were acquired. The lines A, B and C denote the directions of the traces to be shown in other figures. 1 and 2 denote the spots where the ruby spectra in Fig 2 were taken.

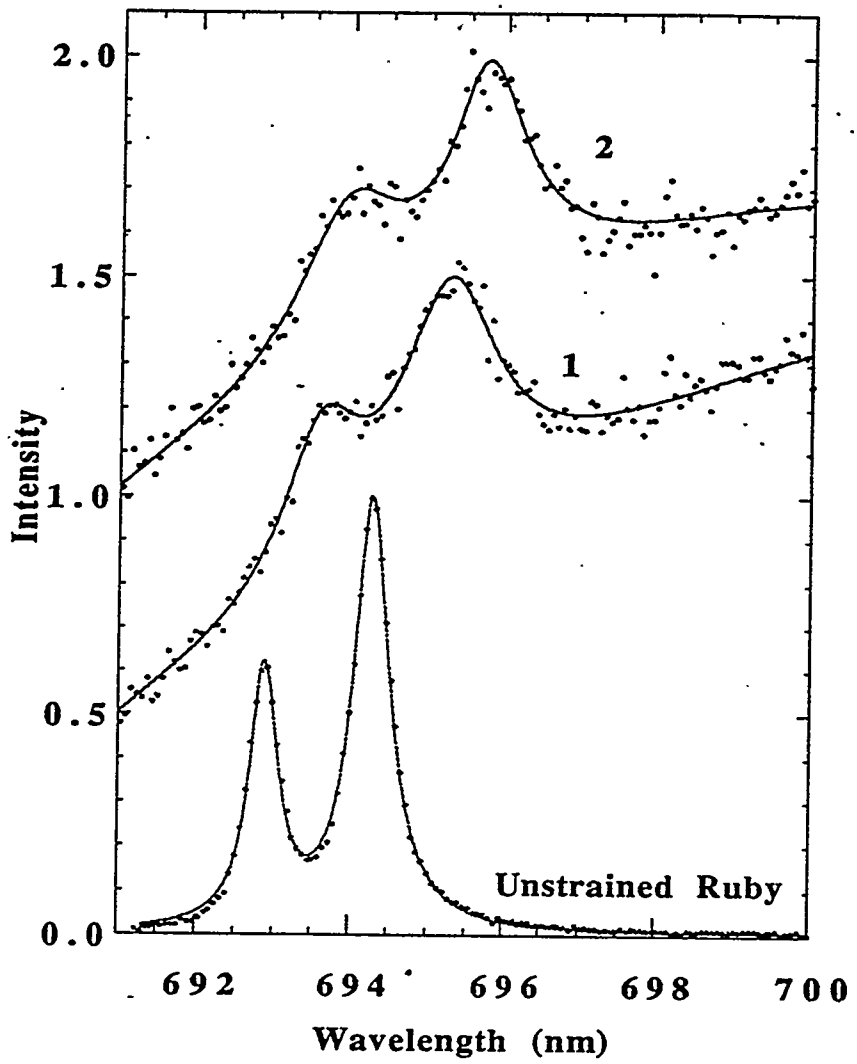

Fig 2. Ruby spectra recorded at spots 1 and 2 in Fig 1 and of a ruby crystal.

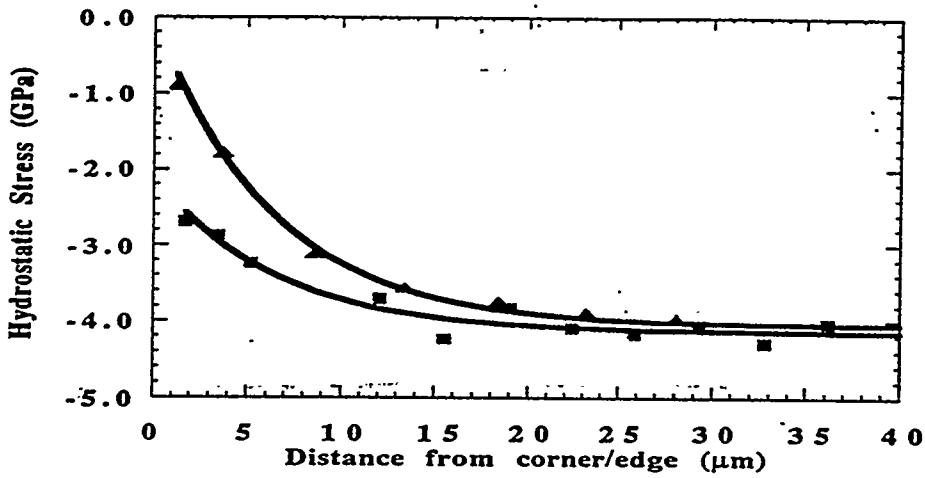

Fig 3 Stress trace along lines B (squares) and C (triangles) of Fig 1. The full lines are fits to Eq. 3.

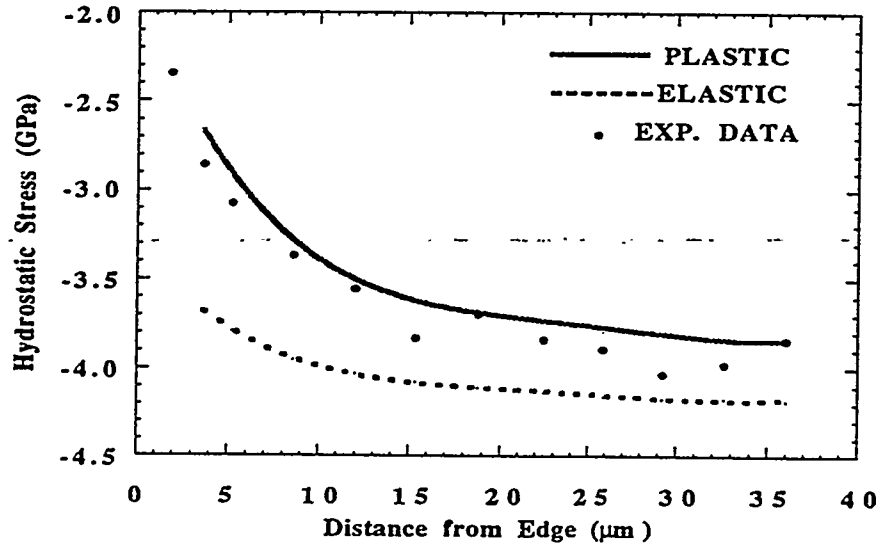

Fig 4 Stress as a function of distance from the sample edge (like along line A of Fig. 1). Symbols are average experimental data collected from multiple samples. Lines are calculated for plastic (full) and elastic (dashed) substrates.